

Supporting Information

Oxidation of Levitated Exo-Tetrahydrodicyclopentadiene Droplets Doped with Aluminum Nanoparticles

Michael Lucas^{1*}, Stephen J. Brotton^{1*}, Ahreum Min¹, Michelle L. Pantoya², Ralf I. Kaiser¹

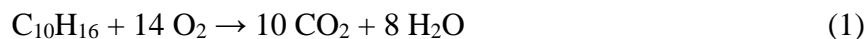
¹Department of Chemistry, University of Hawai'i at Manoa, Honolulu, HI 96822

²Mechanical Engineering Department, Texas Tech University, Lubbock, TX 79409

*Contributed equally to this work.

REACTION YIELDS

H₂O and CO₂ are formed by oxidizing JP-10 through the reaction:



In this section, we will determine the quantities of reactants and products for reaction (1) and the moles of unoxidized aluminum. Our process chamber has a volume of 15.44 L and was filled with 40 ± 1 % of O₂. Therefore, using the ideal gas law, there were 0.2871 ± 0.0053 moles of O₂ before reaction. The Al/JP-10 droplet studied here had a volume of $(4.6 \pm 1.4) \times 10^{-3} \text{ cm}^3$ and contained 99.5 wt. % of JP-10; therefore, using the density of 0.9314 g cm^{-3} for JP-10,¹ it is determined that the unreacted droplet contained $(3.14 \pm 0.92) \times 10^{-5} \text{ mol}$ of JP-10. Since the molar ratio of O₂: JP-10 of 9140:1 is much larger than the stoichiometric ratio of the reactants of 14:1 (see reaction (1)), O₂ is the excess reactant. The FTIR spectrum in Figure 5 did not show evidence for CO, which confirms that O₂ was the excess reactant.

The oxygen can also react with the aluminum; the reaction for the complete oxidation of aluminum is:



The Al/JP-10 droplet contains 0.5 wt. % of Al NPs with an average diameter of 80 nm. The Al NPs have a 4 nm thick Al₂O₃ outer shell that needs to be accounted for when determining the initial quantity of unoxidized Al. The mass ratio of Al to Al₂O₃ in the nanoparticle is therefore 1.839, where we have used 2.90 g cm^{-3} and 3.95 g cm^{-3} for densities of Al and Al₂O₃, respectively. The initial amount of unoxidized aluminum is consequently $(5.16 \pm 0.72) \times 10^{-7} \text{ mol}$.

We can calculate the moles of CO₂ and H₂O produced by comparing the absorbances for CO₂ and H₂O observed in the FTIR spectrum (Figure 5) with the known cross sections. The required absorption cross sections for CO₂ and H₂O were calculating using the *SPECTRA* Information System² and the absorption lines from the HITRAN molecular spectroscopic database.³ The absorption cross sections were calculated for band c of CO₂ centered at 2349 cm^{-1} and for band d of H₂O at 1635 cm^{-1} (Figure 5, Table S3). The FTIR spectra of these bands and the reference absorption cross sections are shown in Figure S7. To calculate the moles of CO₂ and H₂O produced, the Beer-Lambert law was used:

$$A = \frac{n\sigma L}{\text{Log}_e(10)} \quad (3)$$

where A is the absorbance, σ is the absorption cross section, L is the path length of 37.63 cm, and n is the number density of the absorber. At the maximum of band c for CO₂ corresponding to 2362 cm⁻¹, the measured absorbance is 0.283 ± 0.001 and the reference absorption cross section is $(2.608 \pm 0.026) \times 10^{-18}$ cm² molecule⁻¹; therefore, using equation (3), $(1.70 \pm 0.02) \times 10^{-4}$ moles of CO₂ were produced. The quantity of H₂O produced is calculated using the peak at 1653 cm⁻¹, which reaches a maximum absorbance of 0.00887 ± 0.00033 . The reference absorption cross section at the same peak is $(1.186 \pm 0.012) \times 10^{-19}$ cm² molecule⁻¹, and so $(1.173 \pm 0.046) \times 10^{-4}$ mol of H₂O were produced. The molar ratio of CO₂ to H₂O is expected to be 1.25:1, whereas the measured molar ratio is 1.45:1 indicating that slightly less water was detected than expected. This could be caused by water condensing on the surfaces within the stainless-steel chamber. Therefore, we only use the quantity of CO₂ formed to calculate the moles of O₂ and JP-10 consumed. The formation of CO₂ would consume $(2.38 \pm 0.03) \times 10^{-4}$ mol of O₂ and $(1.70 \pm 0.02) \times 10^{-5}$ mol of JP-10. The calculated amount of JP-10 consumed is a factor of 0.54 lower than the initial amount of JP-10 of $(3.14 \pm 0.92) \times 10^{-5}$ mol, which is a consequence of the incomplete combustion of JP-10.

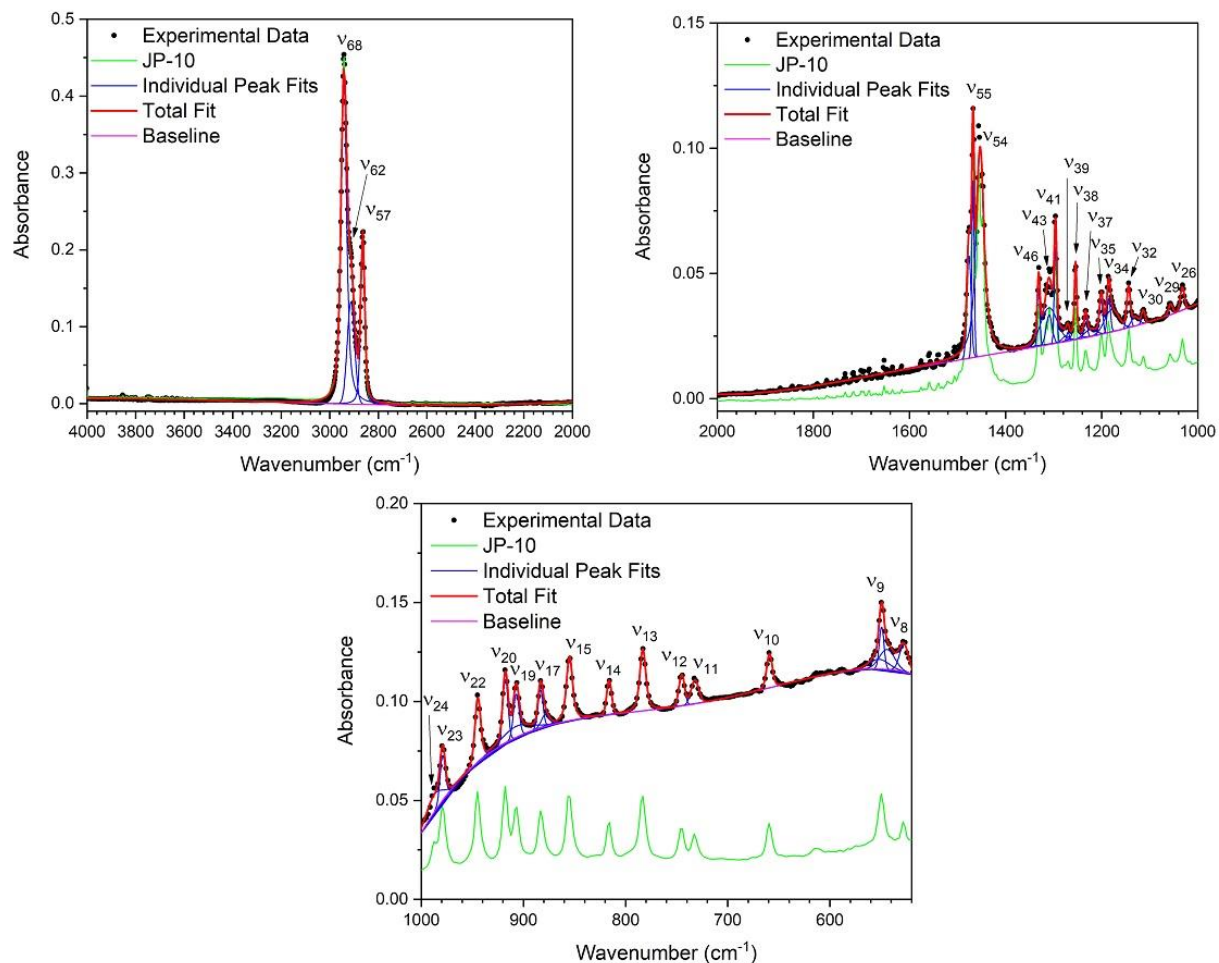


Figure S1. ATR-FTIR spectra of Al/JP-10 with the individual peak fits. FTIR spectra of pure JP-10 (green lines) are shown for comparison. The individual peaks are labelled with $v_{\#}$ and the peak assignments are compiled in Table S2.

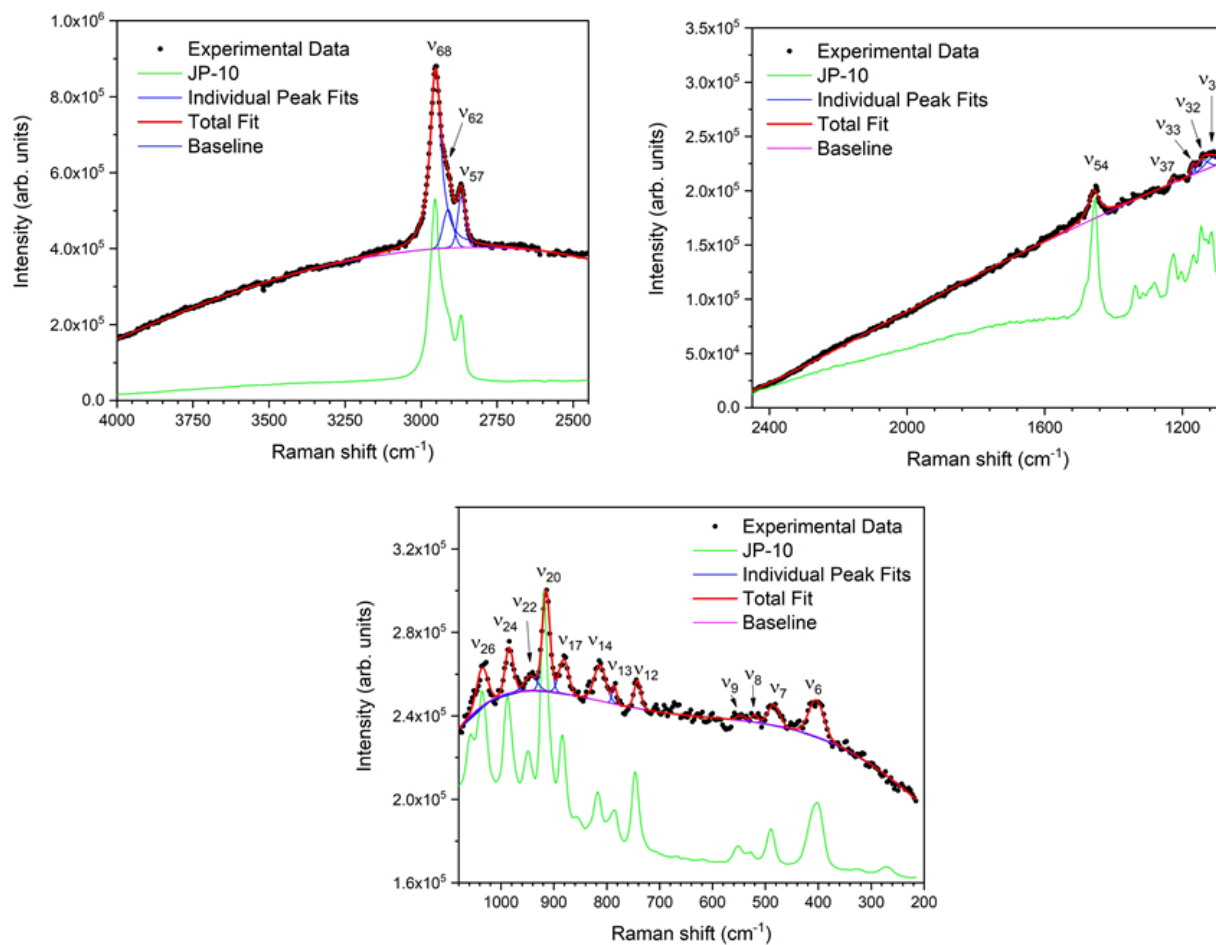


Figure S2. Raman spectra of Al/JP-10 with the individual peak fits. Raman spectra of pure JP-10 (green lines) are shown for comparison. The individual peaks are labelled with v_# and the peak assignments are compiled in Table S2.

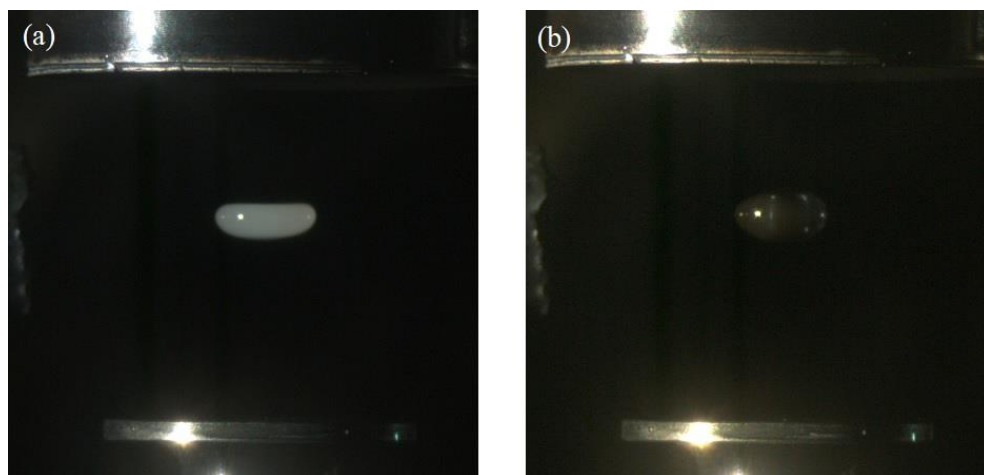


Figure S3. Photographs of a levitated droplet of (a) $\text{Al}_2\text{O}_3/\text{JP-10}$ or (b) $\text{CuO}/\text{JP-10}$.

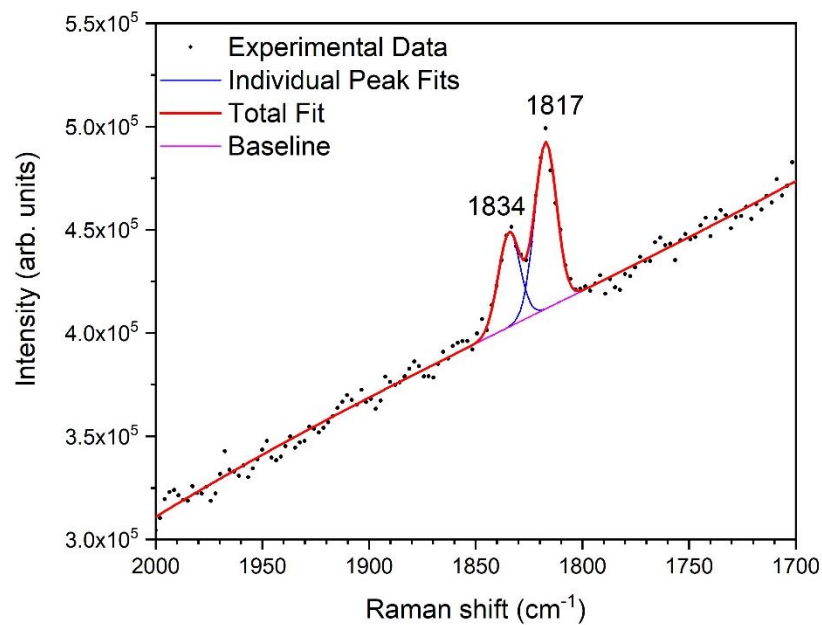


Figure S4. Emission doublet produced by the $^2\text{P}_{3/2,1/2} \rightarrow ^2\text{S}_{1/2}$ transitions of atomic sodium at 589.00 nm and 589.59 nm, respectively, which appears in the Raman spectrum during ignition of an Al/JP-10 droplet levitated in 40% O_2 and 60% Ar.

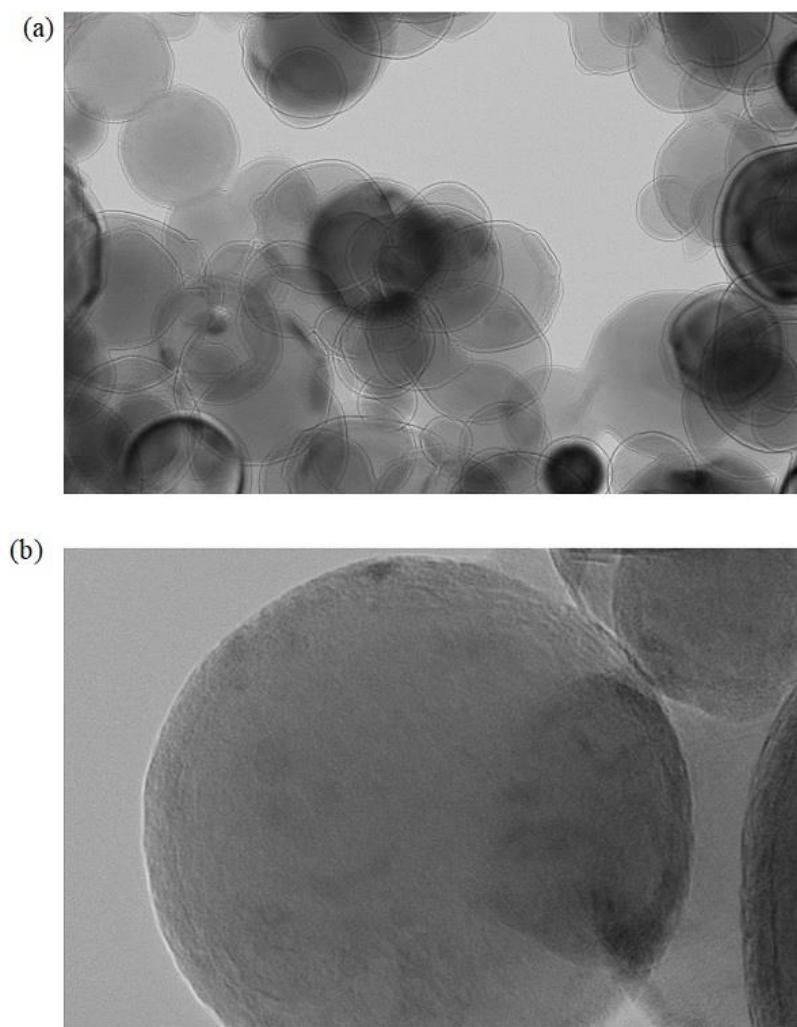


Figure S5. TEM images showing (a) the different sizes of the aluminum nanoparticles and (b) a single particle to display the Al_2O_3 outer shell.

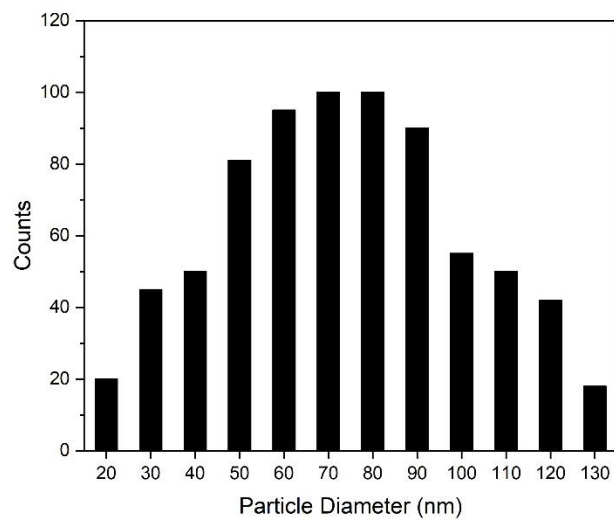


Figure S6. Size distribution of the aluminum nanoparticles. The counts are proportional to the volume of particles with diameters within the specified ranges.

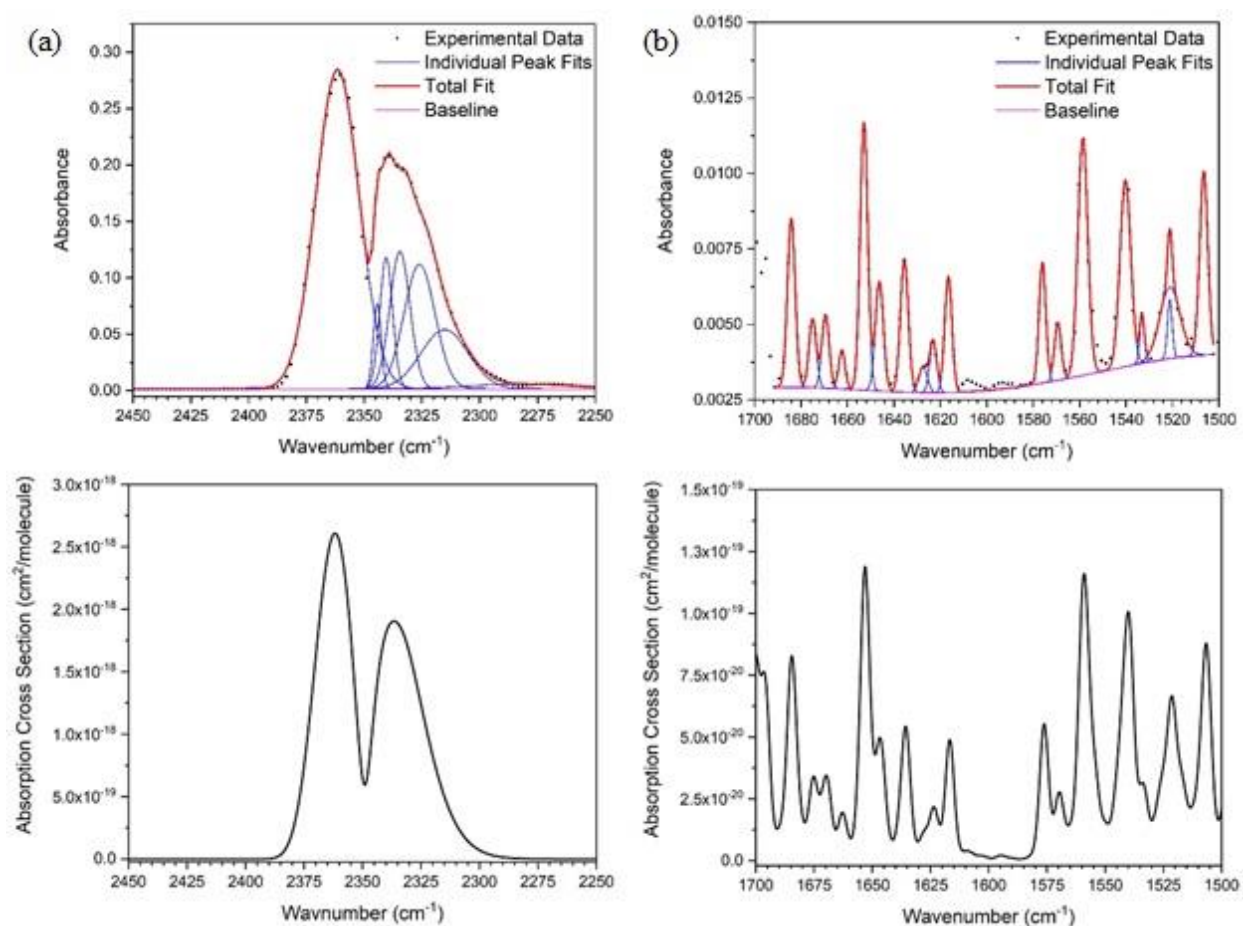


Figure S7. Experimental FTIR spectra (top row) and the reference absorption cross sections (bottom row).² Column (a) shows the 2349 cm⁻¹ absorption band c of CO₂ (Table S3) and column (b) the H₂O absorption band d (Table S4). The spectral resolution was 4 cm⁻¹ in all the Figures.

Table S1. Vibrational Mode Assignments for the Observed Peaks in the FTIR and Raman Spectra of JP-10.

Number	FTIR Wavenumbers (cm ⁻¹) ^a	Raman Wavenumbers (cm ⁻¹) ^a	Calculated Wavenumbers (cm ⁻¹) ^b	Vibrational Mode Assignment
68	2942	2955	3073	CH stretch
62	2913	2912	3042	CH ₂ stretch
57	2865	2868	3016	CH stretch
55	1468	1472 ± 6	1514	CH ₂ scissor
54	1456	1454	1502	CH ₂ scissor
47		1337	1343	CH wag
46	1330		1331	CH ₂ wag
44	1316	1315 ± 3	1317	CH ₂ wag
43	1309		1311	CH ₂ wag
41	1297	1300 ± 8	1301	CH wag
40	1277	1284	1289	CH ₂ wag
39	1270		1261	CH ₂ twist
38	1254		1251	CH ₂ twist
37	1233	1228	1227	CH ₂ rock
35	1201	1202	1205	CH ₂ twist
34	1186		1193	CH ₂ wag
33		1169	1169	CH ₂ twist
32	1144	1145	1153	CH ₂ twist
31	1129 ± 2	1130	1138	CH ₂ twist

Number	FTIR Wavenumbers (cm ⁻¹) ^a	Raman Wavenumbers (cm ⁻¹) ^a	Calculated Wavenumbers (cm ⁻¹) ^b	Vibrational Mode Assignment
30	1113	1115	1073	Rock, CH ₂ twist
29	1057	1057	1054	CH ₂ Wag
26	1032	1035	1041	CH ₂ Twist
24	988	988	992	CC stretch
23	980		963	CC stretch
22	945	948	955	Ring breathing
20	918	919	918	CH ₂ twist
19	907		913	CC stretch
17	883	884	889	CC stretch
15	855	857	863	CCC bend
14	816	817	828	CH ₂ rock
13	783	785	792	CC stretch
12	745	746	753	CC stretch
11	733		739	CCC bend
10	659		671	Ring rock
	613			
9	554	552	554	CCC bend
8	528	527 ± 3	534	Ring twist
7		490	495	CCC bend
6		396	397	CCC bend

^aThe uncertainties are equal to, or less than, 1 cm⁻¹ unless stated otherwise. ^bBased on reference 4.

Table S2. Vibrational Mode Assignments for the Observed Peaks in the FTIR and Raman Spectra of Al/JP-10.

Number	FTIR Wavenumbers (cm⁻¹)^a	Raman Wavenumbers (cm⁻¹)^a	Calculated Wavenumbers (cm⁻¹)^b	Vibrational Mode Assignment
68	2942	2952	3073	CH stretch
62	2913	2911	3042	CH ₂ stretch
57	2864	2868	3016	CH stretch
55	1468		1514	CH ₂ scissor
54	1453	1457	1502	CH ₂ scissor
47		1337	1343	CH wag
46	1331		1331	CH ₂ wag
43	1309 ± 4		1311	CH ₂ wag
41	1296		1301	CH wag
39	1270 ± 18		1261	CH ₂ twist
38	1254		1251	CH ₂ twist
37	1233 ± 2	1228 ± 2	1227	CH ₂ rock
35	1201		1205	CH ₂ twist
34	1185 ± 2		1193	CH ₂ wag
33		1170 ± 2	1169	CH ₂ twist
32	1144	1141 ± 23	1153	CH ₂ twist
30	1113 ± 4	1108 ± 71	1073	CH ₂ Rock, twist
29	1056 ± 2		1054	CH ₂ Wag
26	1032	1036	1041	CH ₂ Twist
24	987	984	992	CC stretch
23	979		963	CC stretch
22	945	944 ± 2	955	Ring breathing

Number	FTIR Wavenumbers (cm⁻¹)^a	Raman Wavenumbers (cm⁻¹)^a	Calculated Wavenumbers (cm⁻¹)^b	Vibrational Mode Assignment
20	918	915	918	CH ₂ twist
19	907		913	CCC stretch
17	883 ± 2	881	889	CC stretch
15	855		863	CCC bend
14	816	812	828	CH ₂ rock
13	783	785	792	CC stretch
12	745	741	753	CC stretch
11	732		739	CCC bend
10	659		671	Ring rock
9	549	545 ± 6	554	CCC bend
8	528	520 ± 4	534	Ring twist
7		484	495	CCC bend
6		404	397	CCC bend

^aThe uncertainties are equal to, or less than, 1 cm⁻¹ unless stated otherwise.

^bBased on reference ⁴.

Table S3. Assignment of the vibrational modes in the FTIR spectra collected following oxidation of Al/JP-10.

Band	Experimental band center (cm ⁻¹)	Reference band center (cm ⁻¹)	Molecule	Number (symmetry)	Vibrational Mode	Ref.
a	3714	3715	CO ₂	$\nu_1(\sigma_g^+) + \nu_3(\sigma_u^+)$	Combination band	5
b	3612	3613	CO ₂	$\nu_1(\sigma_g^+) + \nu_3(\sigma_u^+)$	Combination band	5
c	2349	2349	CO ₂	$\nu_3(\sigma_u^+)$	CO ₂ asym. str.	5
d	1635	1635	H ₂ O	$\nu_2(A')$	OH bend	6
e	669	667	CO ₂	$\nu_2(\pi_u)$	CO ₂ bend	5

Movie M1. High-speed video of an igniting Al/JP-10 droplet.

REFERENCES

- (1) Bruno, T. J.; Huber, M. L.; Laesecke, A.; Lemmon, E. W.; Perkins, R. A., Thermochemical and Thermophysical Properties of JP-10. **2006**, *6640*, 325.
- (2) Mikhailenko, C. N.; Babikov, Y. L.; Golovko, V. F., Information-Calculating System Spectroscopy of Atmospheric Gases. The Structure and Main Functions. *J Atmos. Oceanic Opt.* **2005**, *18*, 685-695.
- (3) Gordon, I. E.; Rothman, L. S.; Hill, C.; Kochanov, R. V.; Tan, Y.; Bernath, P. F.; Birk, M.; Boudon, V.; Campargue, A.; Chance, K. V.; Drouin, B. J.; Flaud, J. M.; Gamache, R. R.; Hodges, J. T.; Jacquemart, D.; Perevalov, V. I.; Perrin, A.; Shine, K. P.; Smith, M. A. H.; Tennyson, J.; Toon, G. C.; Tran, H.; Tyuterev, V. G.; Barbe, A.; Csaszar, A. G.; Devi, V. M.; Furtenbacher, T.; Harrison, J. J.; Hartmann, J. M.; Jolly, A.; Johnson, T. J.; Karman, T.; Kleiner, I.; Kyuberis, A. A.; Loos, J.; Lyulin, O. M.; Massie, S. T.; Mikhailenko, S. N.; Moazzen-Ahmadi, N.; Muller, H. S. P.; Naumenko, O. V.; Nikitin, A. V.; Polyansky, O. L.; Rey, M.; Rotger, M.; Sharpe, S. W.; Sung, K.; Starikova, E.; Tashkun, S. A.; Vander Auwera, J.; Wagner, G.; Wilzewski, J.; Wcislo, P.; Yu, S.; Zak, E. J., The HITRAN2016 Molecular Spectroscopic Database. *J. Quant. Spectrosc. Radiat. Transfer* **2017**, *203*, 3-69.
- (4) Morozov, A. N.; Mebel, A. M.; Kaiser, R. I., A Theoretical Study of Pyrolysis of exo-Tetrahydrodicyclopentadiene and Its Primary and Secondary Unimolecular Decomposition Products. *J. Phys. Chem. A* **2018**, *122*, 4920-4934.
- (5) Miller, C. E.; Brown, L. R., Near Infrared Spectroscopy of Carbon Dioxide I. $^{16}\text{O}^{12}\text{C}^{16}\text{O}$ Line Positions. *J. Mol. Spectrosc.* **2004**, *228*, 329-354.
- (6) Zou, Q.; Varanasi, P., Laboratory Measurement of the Spectroscopic Line Parameters of Water Vapor in the 610-2100 and 3000-4050 cm^{-1} Regions at Lower-Tropospheric Temperatures. *J. Quant. Spectrosc. Radiat. Transfer* **2003**, *82*, 45-98.